Monostatic Sensing for Passive RIS Localization and Tracking

Zi Ye, Faryal Junaid, Emad Ibrahim, Rickard Nilsson, and Jaap van de Beek, *Fellow, IEEE*

***Abstract*—Reconfigurable intelligent surfaces (RIS) have emerged as a promising technology for 6G networks. In this letter, we explore a novel use case for RIS: passive localization and tracking of a RIS-equipped object using monostatic sensing, where the fixed transmitter and receiver share the same single antenna, using OFDM signals. We develop a low-complexity algorithm that achieves centimeter-level accuracy using only 6 MHz bandwidth, and by applying temporal coding to random RIS phase profiles, separating signals from undesired multipath sources. In addition, we evaluate the impact of model uncertainty on the performance of the algorithm.**

***Index Terms*—Reconfigurable intelligent surface, passive localization, tracking, extended Kalman filter.**

I. Introduction

INDOOR localization and tracking have become increasingly important in recent years due to the growing need for efficient and accurate navigation solutions in various applications such as smart homes, robotics, and IoT devices. Traditional indoor localization systems often rely on multiple antennas and an array of sensors, resulting in a complex and costly infrastructure. However, the rapid advancement in RIS has opened new possibilities for more efficient and cost-effective solutions [1].

RISs are planar structures engineered to manipulate electromagnetic waves in a controlled manner, which can be leveraged to enhance the performance of monostatic sensing systems. By dynamically adjusting the RIS configuration, one can optimize its interaction with incoming signals, ultimately enhancing localization precision and tracking capabilities. Besides these benefits, RISs are semi-passive, low-cost devices, making them ideally suited for installation on both static surfaces and moving objects.

Considering the characteristics of the user, localization techniques can be divided into active and passive methods. In the former, the user either transmits or receives signals [2], [3], while in the latter, the user merely reflects or scatters signals from a transmitter [4], [5]. The authors in [6] introduce a novel full-duplex UE self-localization method where a RIS is used to reflect the signal transmitted by the UE back to the UE itself. Some studies have been conducted on tracking the user, [7] proposes a Bayesian user localization and tracking algorithm for multiple RISs-aided mmWave MIMO systems in an online fashion, [8] investigates a multiple RISs-aided single-user MIMO scenario, utilizing an Extended Kalman Filter (EKF) for user trajectory tracking and analyzing the impact of positioning on communication performance in non-line-of-sight conditions. Reference [9] explores the use of RIS to replace remote cells in downlink time-difference-of-arrival measurements for positioning within a single cell, employing an EKF algorithm for user tracking.

In this letter, we investigate a novel approach for indoor passive RIS localization and tracking, where a single-antenna full-duplex transceiver forms a monostatic sensing system that transmits signals and receives the reflected signals from the object equipped with a RIS, as well as other scatterers in the environment. Our main contributions can be summarized as follows: i) We formulate the system model for multicarrier transmission, taking into account the unknown multipath effects from the environment. By designing an appropriate RIS phase profile, we could eliminate multipath interference. ii) We propose a novel low-complexity RIS location estimator and an EKF tracking algorithm that could track the speed and location of the object. iii) We evaluate the performance of the proposed methods in terms of estimation accuracy through simulations in different indoor environments.

Notations: Hermitian, transpose, conjugate, and pseudoinverse of the matrix are represented by $()^{\mathrm{H}}$, $()^{\top}$, $()^{*}$ and $()^{\dagger}$, $\cdot$ denotes the dot product, $\|\|$ and $\|\|_F$ indicates the modulus and the frobenius norm, and $j^2 = -1$. The real and imaginary parts are indicated by $\Re$ and $\Im$.

II. System Model

We consider a wireless system as depicted in Fig. 1 comprising of a single-antenna, full-duplex transceiver with a known location $\mathbf{p}_0 \in \mathbb{R}^3$ and an object with an unknown location $\mathbf{p}_r \in \mathbb{R}^3$ in the plane $z = 0$, equipped with a RIS. We assume that $\mathbf{p}_r$ represents the center location of the RIS, which is to be estimated, and $\mathbf{p}_{r,m} \in \mathbb{R}^3$ represents the location of the mth RIS element. Therefore, the center RIS location relative to the transceiver can be expressed as $\mathbf{p}_{0r} = \mathbf{p}_0 - \mathbf{p}_r$. The RIS adopts the form of a Uniform Planar Array (UPA) containing M elements with inter-element spacing of $\frac{\lambda}{4}$ [6], where λ represents the signal wavelength.

The transceiver transmits L consecutive OFDM symbols on N subcarriers with frequency spacing Δ_f, and receives the reflected signals from the RIS and other scatterers in the environment. We assume that the energy of all transmitted symbols is P_t. At the transceiver, the received signal over time

Manuscript received 7 October 2023; revised 23 January 2024; accepted 13 February 2024. Date of publication 19 February 2024; date of current version 10 May 2024. This work was supported in part by the European SNS-JU Project Hexa-X-II under Grant 101095759, and in part by the European Interreg Aurora Project Arctic-6G. The associate editor coordinating the review of this article and approving it for publication was B. Tan. *(Corresponding author: Zi Ye.)*

The authors are with the Department of Computer Science, Electrical and Space Engineering, Luleå University of Technology, 97187 Luleå, Sweden (e-mail: zi.ye@ltu.se; faryal.junaid@ltu.se; emad.farouk.ibrahim@ltu.se; rickard.o.nilsson@ltu.se; jaap.vandebeek@ltu.se).

Digital Object Identifier 10.1109/LWC.2024.3367528

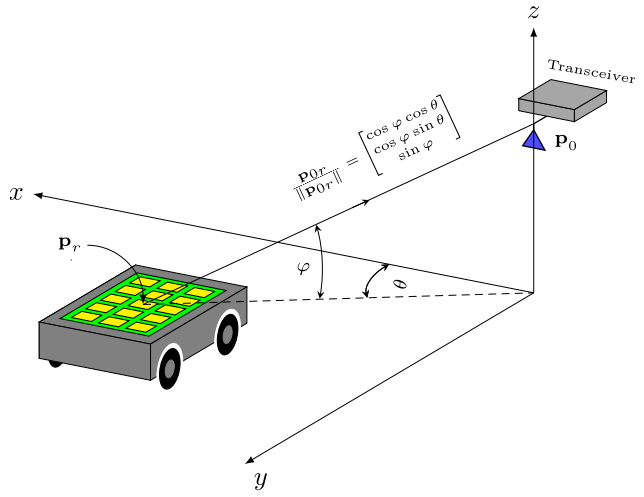

Fig. 1. System setup with a single antenna transceiver at a known location $\mathbf{p}_0$, and an object equipped with a RIS, with unknown location and velocity to be estimated, moving in the plane $z = 0$.

and subcarriers is given by the matrix $\mathbf{Y} \in \mathbb{C}^{N\times L}$ [6]

$$\mathbf{Y} = \sqrt{P_t} g_{0r}\mathbf{d}(\tau_{0r})\mathbf{b}^\top \mathbf{\Omega} + \sqrt{P_t}\sum_{s=1}^{N_s} g_{0s}\mathbf{d}(\tau_{0s})\mathbf{1}_L^\top + \mathbf{W}, \quad (1)$$

where $g_{0r} = \rho_{0r}e^{j\psi}$ is the complex channel gain with unknown global phase offset $\psi \sim \mathcal{U}[0, 2\pi)$ due to the lack of phase synchronization between the different entities, and attenuation amplitude ρ_{0r} given by [10], [11]

$$\rho_{0r} = \frac{\left(\frac{\lambda}{4}\right)^2 (\sin\varphi)^{2q_0}}{4\pi\|\mathbf{p}_{0r}\|^2}, \quad (2)$$

where φ is the elevation angle from the center of the RIS to the transceiver and $q_0 = 0.285$ [10]. Furthermore in (1), the transmission delay τ_{0r} is given by

$$\tau_{0r} = \frac{2\|\mathbf{p}_{0r}\|}{c} = \frac{2[\mathbf{p}_0]_3}{c\sin\varphi}, \quad (3)$$

where c is the speed of light, and the phase offset produced by the delay on each subcarrier is denoted as $\mathbf{d}(\tau)$

$$\mathbf{d}(\tau) = \left[1, e^{-j2\pi\tau\Delta_f}, \ldots, e^{-j2\pi\tau(N-1)\Delta_f}\right]^\top. \quad (4)$$

The vector $\mathbf{b} \in \mathbb{C}^M$ is the RIS response vector, given by

$$[\mathbf{b}]_m = e^{-j2\frac{2\pi}{\lambda}(\|\mathbf{p}_0 - \mathbf{p}_{r,m}\| - \|\mathbf{p}_{0r}\|)}. \quad (5)$$

In the far-field assumption, the factor in the exponent of (5), $\|\mathbf{p}_0 - \mathbf{p}_{r,m}\| - \|\mathbf{p}_{0r}\|$ can be approximated as $\mathbf{q}_m^\top \frac{\mathbf{p}_{0r}}{\|\mathbf{p}_{0r}\|}$, where $\mathbf{q}_m = r_m[\cos(\xi_m + \alpha)\ \sin(\xi_m + \alpha)\ 0]^\top \in \mathbb{R}^3$, in which r_m (resp. ξ_m) denotes the RIS mth element's distance (resp. azimuth angle) from the origin, α is the orientation of the RIS planar in the plane $z = 0$ which is assumed to be known. The wave vector $\frac{\mathbf{p}_{0r}}{\|\mathbf{p}_{0r}\|}$ is indicated in Fig. 1. Thus, the RIS response vector $\mathbf{b}$ is a function of θ and φ, and (5) can be rewritten as

$$[\mathbf{b}(\theta,\varphi)]_m = e^{-j2\frac{2\pi}{\lambda} r_m \cos\varphi\cos(\theta-\alpha-\xi_m)}. \quad (6)$$

The number of unknown and unwanted multipaths is given by N_s, each path's path loss and delay are denoted by g_{0s} and τ_{0s}. Here, we assume that the wavelength remains constant across the entire transmission bandwidth, allowing us to neglect beam squint effects [5]. We ignore the Doppler effect in this letter, as it may not be a critical factor considering a slowly moving object that causes a negligible frequency shift. We further assume that the RIS is managed by a controller which modulates the phase of the incident wave according to the RIS phase profile matrix $\mathbf{\Omega} = \exp(j\boldsymbol{\omega}) \in \mathbb{C}^{M\times L}$ on each element which changes over time. The noise matrix $\mathbf{W} \in \mathbb{C}^{N\times L}$ has i.i.d circularly-symmetric Gaussian elements with variance σ^2.

Finally, we choose the RIS phase profile $\mathbf{\Omega}$ with a particular structure and we assumem that $\mathbf{\Omega}$ is fully known to the transceiver. Inspired by the design of this profile in [6], we study to remove the unknown multipath reflected by the scatterers from the received signal in (1). We divide the number of transmissions L in half, and denote them by $L_1 = 1, 2, \ldots, \frac{L}{2}$ and $L_2 = \frac{L}{2} + 1, \ldots, L$, the corresponding phase profile is denoted by $\mathbf{\Omega}_1 = \tilde{\mathbf{\Omega}} = \exp(j\tilde{\boldsymbol{\omega}}) \in \mathbb{C}^{M\times\frac{L}{2}}$ and $\mathbf{\Omega}_2 = -\tilde{\mathbf{\Omega}}$. Each entry of the matrix $\mathbf{\Omega}_1$ is randomly and independently drawn from the unit circle. Thus, the received signal in (1) can also be divided into $\mathbf{Y}_1$ and $\mathbf{Y}_2$, both $\in \mathbb{C}^{N\times\frac{L}{2}}$.

Our goal is to estimate the location and velocity of the moving object equipped with a RIS, using low complexity methods based on the observation $\mathbf{Y}$, given the fixed location of the transceiver and the RIS phase profile.

III. Low Complexity Location Estimator

The receiver, in the first step, computes the following quantity $\tilde{\mathbf{Y}} \in \mathbb{C}^{N\times\frac{L}{2}}$ as the new observation

$$\tilde{\mathbf{Y}} = \frac{1}{2}(\mathbf{Y}_1 - \mathbf{Y}_2) = \sqrt{P_t} g_{0r}\mathbf{d}(\tau_{0r})\mathbf{b}^\top\tilde{\mathbf{\Omega}} + \tilde{\mathbf{W}}, \quad (7)$$

where the noise matrix $\tilde{\mathbf{W}} \sim \mathcal{N}(0, \frac{\sigma^2}{2}) \in \mathbb{C}^{N\times\frac{L}{2}}$. By doing so, the unknown and undesired multipath are removed.

Using the Jacobi-Anger identity [2], (6) can be written as

$$[\mathbf{b}(\theta,\varphi)]_m \approx \sum_{i=-I}^{I} j^i \mathrm{J}_i\left(-\frac{4\pi}{\lambda} r_m\cos(\theta-\alpha-\xi_m)\right)\exp(ji\varphi), \quad (8)$$

where J_i is the ith order Bessel functions of the first kind. Thus, (6) can be further rewritten as $\mathbf{b}(\theta,\varphi) = \mathbf{G}(\theta)\mathbf{F}(\varphi)$, where $\mathbf{G}(\theta) \in \mathbb{C}^{M\times I}$ with each entity $[\mathbf{g}_m(\theta)]_i = j^i\mathrm{J}_i(-\frac{4\pi}{\lambda} r_m\cos(\theta-\alpha-\xi_m))$, and $[\mathbf{F}(\varphi)]_i = \exp(ji\varphi)$. In this manner, $\mathbf{b}(\theta,\varphi)$ is in a form separable at angles θ and φ.

Since the transmission delay τ_{0r} is a function of φ according to (3), we can rewrite (7),

$$\tilde{\mathbf{Y}} = \sqrt{P_t} g_{0r}\mathbf{d}(\varphi)\mathbf{F}(\varphi)^\top\mathbf{G}(\theta)^\top\tilde{\mathbf{\Omega}} + \tilde{\mathbf{W}}. \quad (9)$$

such that the maximum likelihood estimation becomes

$$\left[\hat{g}_{0r}, \hat{\theta}, \hat{\varphi}\right] = \arg\min_{g_{0r},\theta,\varphi}\left\|\tilde{\mathbf{Y}} - \sqrt{P_t} g_{0r}\mathbf{d}(\varphi)\mathbf{F}(\varphi)^\top\mathbf{G}(\theta)^\top\tilde{\mathbf{\Omega}}\right\|_F^2. \quad (10)$$

Now that the angles θ and φ are in independent form in (10), we can operate a 2-stage 1D search estimator, which is less complex than a 2D joint search.

In a first stage, we estimate the angle φ: after introducing $\gamma = \sqrt{P_t} g_{0r} \mathbf{G}(\theta)^\top \tilde{\mathbf{\Omega}} \in \mathbb{C}^{I \times \frac{L}{2}}$, we apply a least mean square method to express γ as a function of φ, $\hat{\gamma}(\varphi) = \frac{1}{N}(\mathbf{F}(\varphi)^* \mathbf{F}(\varphi)^\top)^\dagger \mathbf{F}(\varphi)^* \mathbf{d}(\varphi)^{\mathrm{H}} \tilde{\mathbf{Y}}$. Thus, the estimation of angle φ can be obtained by a 1D search as

$$\hat{\varphi} = \arg\min_{\varphi} \left\| \tilde{\mathbf{Y}} - \mathbf{d}(\varphi) \mathbf{F}(\varphi)^\top \hat{\gamma}(\varphi) \right\|_F^2. \tag{11}$$

In a second stage, we estimate the angle θ: with the angle $\hat{\varphi}$ estimated in the previous step, by introducing $\eta(\theta) = \mathbf{d}(\hat{\varphi}) \mathbf{F}(\hat{\varphi})^\top \mathbf{G}(\theta)^\top \tilde{\mathbf{\Omega}} \in \mathbb{C}^{N \times \frac{L}{2}}$ and using the least mean square method, the complex channel gain can be expressed as $\hat{g}_{0r}(\theta) = \|(\eta(\theta)^{\mathrm{H}} \eta(\theta))^\dagger \eta(\theta)^{\mathrm{H}} \tilde{\mathbf{Y}} / \sqrt{P_t}\|_F^2$. Hence, the estimation of angle θ can be obtained by a 1D search as

$$\hat{\theta} = \arg\min_{\theta} \left\| \tilde{\mathbf{Y}} - \sqrt{P_t} \hat{g}_{0r}(\theta) \eta(\theta) \right\|_F^2. \tag{12}$$

IV. Tracking With an Extended Kalman Filter

The Extended Kalman Filter (EKF) is a widely used recursive algorithm for tracking the motion of an object. Its widespread use is due to its ability to handle system nonlinearities and its effectiveness with noisy observations.

We consider the scenario where the object follows the constant velocity motion model [12], and define the state vector at time step k for this model as

$$\boldsymbol{s}_k \in \mathbb{R}^5 = [x_k, \dot{x_k}, y_k, \dot{y_k}, \alpha_k]^\top, \tag{13}$$

where x_k and y_k are the location coordinates, $\dot{x}_k$ and $\dot{y}_k$ are the velocity components in the x and y directions, and α_k is the orientation of the object.

However, in real world, there may be unpredictable forces acting on the model that cause velocity fluctuations that can be modeled as random acceleration. To account for this, the state transition function can be written as [12], [13]

$$\boldsymbol{s}_{k+1} = F \boldsymbol{s}_k + \boldsymbol{w}_k, \quad \text{where} \tag{14}$$

$$F = \begin{bmatrix} 1 & T_s & 0 & 0 & 0 \\ 0 & 1 & 0 & 0 & 0 \\ 0 & 0 & 1 & T_s & 0 \\ 0 & 0 & 0 & 1 & 0 \\ 0 & 0 & 0 & 0 & 1 \end{bmatrix}. \tag{15}$$

The time between successive observations is denoted by T_s, and the process noise $\boldsymbol{w}_k$ represents the uncertainties in the system's motion that cannot be modeled deterministically. Assuming that the object undergoes a random acceleration in velocity in x (resp. y) direction of a_{x_k} (resp. a_{y_k}) $\sim \mathcal{N}(0, \sigma_a^2)$, and random noise in orientation $a_\alpha \sim \mathcal{N}(0, \sigma_\alpha^2)$ between time step $k-1$ and k. From Newton's laws of motion, we have

$$\boldsymbol{w}_k = \left[\frac{T_s^2}{2} a_{x_k}, T_s a_{x_k}, \frac{T_s^2}{2} a_{y_k}, T_s a_{y_k}, a_{\alpha_k} \right]^\top. \tag{16}$$

As a result, the process noise covariance matrix is given by $Q = \mathbb{E}(\boldsymbol{w}_k \boldsymbol{w}_k^\top)$ [12], [13].

To define the observation function, we begin by removing the delay effects from the received signal $\tilde{\mathbf{Y}}$, given by

$$\boldsymbol{y} = \left(\mathbf{d}(\hat{\tau}_{0r})^{\mathrm{H}} \tilde{\mathbf{Y}} \right)^\top \approx N \sqrt{P_t} g_{0r} \tilde{\mathbf{\Omega}}^\top \mathbf{b} + \boldsymbol{v}. \tag{17}$$

We can rewrite (17) as the observation $\boldsymbol{y}_k \in \mathbb{C}^{\frac{L}{2} \times 1}$ at time k

$$\boldsymbol{y}_k = \boldsymbol{h}(\boldsymbol{s}_k) + \boldsymbol{v}_k, \tag{18}$$

where $\boldsymbol{v}_k$ is the observation noise, and its covariance matrix is diagonal represented by R with all entries equal to $N \frac{\sigma^2}{2}$.

The EKF algorithm consists of two main steps: prediction and update. In the prediction step, the algorithm first calculates the predicted state for the current time step k as

$$\hat{\boldsymbol{s}}_{k|k-1} = F \hat{\boldsymbol{s}}_{k-1|k-1}. \tag{19}$$

Then, it computes the predicted error covariance matrix for the current time step k as

$$\hat{\mathbf{P}}_{k|k-1} = F \hat{\mathbf{P}}_{k-1|k-1} F^\top + Q. \tag{20}$$

During the update step, the state estimate and error covariance matrix are adjusted according to

$$\mathbf{K}_k = \hat{\mathbf{P}}_{k|k-1} \mathbf{H}_k^\top \left(\mathbf{H}_k \hat{\mathbf{P}}_{k|k-1} \mathbf{H}_k^\top + R \right)^{-1}, \tag{21}$$

$$\boldsymbol{e}_k = \boldsymbol{y}_k - \boldsymbol{h}\left(\hat{\boldsymbol{s}}_{k|k-1} \right), \tag{22}$$

$$\hat{\boldsymbol{s}}_{k|k} = \hat{\boldsymbol{s}}_{k|k-1} + \mathbf{K}_k [\Re(\boldsymbol{e}_k); \Im(\boldsymbol{e}_k)], \tag{23}$$

$$\hat{\mathbf{P}}_{k|k} = \hat{\mathbf{P}}_{k|k-1} - \mathbf{K}_k \mathbf{H}_k \hat{\mathbf{P}}_{k|k-1}, \tag{24}$$

where $\mathbf{K}_k$ is the Kalman gain, $\mathbf{H}_k = \frac{\partial \boldsymbol{h}}{\partial \boldsymbol{s}} \big|_{\hat{\boldsymbol{s}}_{k|k-1}}$ is the Jacobian matrix of the observation function evaluated at the predicted state estimate, given in detail in the Appendix.

The proposed localization and EKF tracking algorithm can be summarized as follows:

- At time step $k = 0$, the location estimator described in Section III is used to perform localization, initializing the object's estimated location in the state vector $\hat{\boldsymbol{s}}_{0|0}$. The velocity components in the state vector $\hat{\boldsymbol{s}}_{0|0}$ and the error covariance matrix $\hat{\mathbf{P}}_{0|0}$ are both initialized to 0.
- After time step $k \geq 1$, once the prediction and update steps are completed as described in (19)-(24), the EKF has a new state estimate and covariance matrix for the current time step. This process can be repeated for subsequent time steps to track the state of the system.

V. Simulation Results

Simulation Parameters. In our simulations, we model a room with dimensions 8 m × 8 m × 4 m, the object moves on the plane $z = 0$ m, its location is denoted by $\mathbf{p}_r = [x, y, 0]^\top$, where x and y are both in the range $[-4, 4]$ m. T_s is 0.2 sec and the object starts from $[-3, -3, 0]^\top$ at time step $k = 0$, The search resolution of angle φ and θ in (11) and (12) is $\frac{\pi}{90}$. From time steps $k = 1$ to $k = 60$, the object moves with a speed of $\dot{x}_k = 0$ m/sec and $\dot{y}_k = 0.5$ m/sec. From time steps $k = 61$ to $k = 120$, the object moves with a speed of $\dot{x}_k = 0.5$ m/sec and $\dot{y}_k = 0$ m/sec. With a total system bandwidth of 6 MHz, we simulate over 5000 random RIS phase profiles and

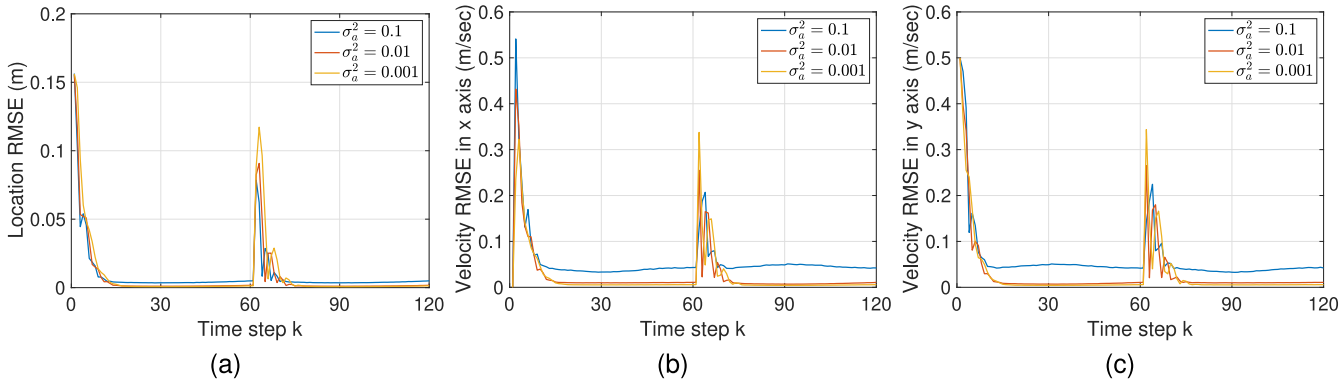

Fig. 2. Process noise $\sigma_a^2 = 0.1, 0.01, 0.001$. Orientation process noise $\sigma_\alpha^2 = 0$. (a) Location RMSE (meter). (b) Velocity RMSE in x axis (meter/sec). (c) Velocity RMSE in y axis (meter/sec).

TABLE I
SIMULATION PARAMETERS

Parameter	Symbol	Value
Wavelength	λ	1 cm
Light speed	c	3×10^8 m/s
Subcarrier bandwidth	Δ_f	120 kHz
Number of subcarriers	N	50
Total transmission power	$N\Delta_f P_t$	30 dBm
Number of transmissions	L	100
Noise power spectral density	N_0	-174 dBm/Hz
UE's noise figure	n_f	3 dB
Noise variance	$\sigma^2 = n_f N_0$	-171 dBm/Hz
Transceiver location	$\mathbf{p}_0$	$[0, 0, 4]^\top$
Jacobi-Anger identity order	I	20

noise realizations to evaluate the performance. The rest of the simulation parameters are given in Table I.

The estimation complexity is determined by the Jacobi-Anger identity order I and the angular search resolution in both φ and θ. To ensure a fair comparison between 1D and 2D searches, we evaluate location estimation at the initial location $[-3, -3, 0]^\top$. In terms of MATLAB runtime for one Mont-Carlo simulation, a 2-stage 1D search takes about 6 seconds, while a 2D search requires about 16 seconds to achieve similar estimation performance. Therefore, the 2-stage 1D search proves to be a more time-efficient choice.

Velocity process noise σ_a^2. An important factor affecting the tracking performance of the system is the velocity process noise σ_a^2, which represents the disturbances in the state transition model. Fig. 2 shows the root mean square error (RMSE) performance of location and velocity in x and y axes over different velocity process noise. When σ_a^2 is small, it indicates that the system is relatively stable, with minimal uncertainty during state transitions. As a result, the EKF's state predictions will be more accurate, leading to better tracking performance. However, if there is a sharp turn in the actual system (e.g., the object changes direction at time step $k = 61$), a small σ_a^2 can cause the EKF to adapt more slowly to these changes. This is because the EKF may take longer to converge to the true state since it has more confidence in the state transition model than in the observations, which may not accurately represent the changes. When σ_a^2 is large, it indicates that the system is believed to have significant uncertainties during state transitions, so the EKF will have less confidence in its predictions and rely more heavily on noisy observations,

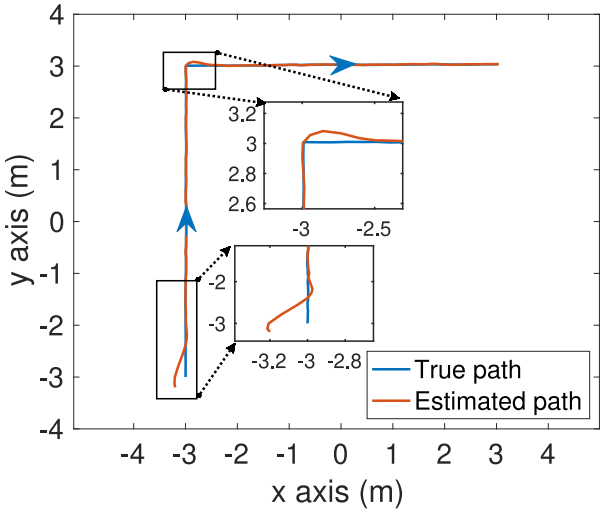

Fig. 3. Velocity process noise $\sigma_a^2 = 0.01$. One example of the trajectory of the true path and the estimated one, starting point at $[-3, -3, 0]^\top$.

which can lead to inaccurate state estimates, but it can also adapt quickly to sharp turns. Fig. 3 shows an example of the trajectory of the true path and the estimated one.

Orientation process noise σ_α^2. While it is assumed that the initial orientation α is known and remains constant during motion according to (13) - (15), it may fluctuate as the object moves. These variations can significantly affect the tracking performance of the system, especially due to the high sensitivity of the channel model to the orientation shown in (6), since there is only a single antenna on the transceiver. Fig. 4 shows that as the degree of orientation change increases, there is a corresponding degradation in tracking performance.

Comparison with other method. The proposed method is contrasted with a 2-stage 1D search location estimation at each time step, as detailed in Section III, and depicted in Fig. 5. It can be seen that the RMSE doesn't converge over time without performing EKF. The EKF plays a crucial role in continuously updating and refining the estimate by incorporating new measurements in an iterative and adaptive process. Notably, the proposed method could accurately estimate the velocity while it could not without the EKF. In terms of runtime efficiency, the proposed method completes one Mont-Carlo simulation with 120 time steps in 8 seconds, while the compared method

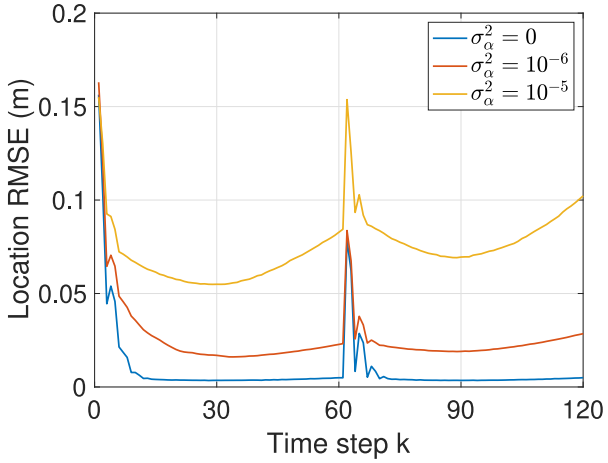

Fig. 4. Velocity process noise $\sigma_a^2 = 0.1$. Location RMSE (meter) with different orientation process noise σ_α^2.

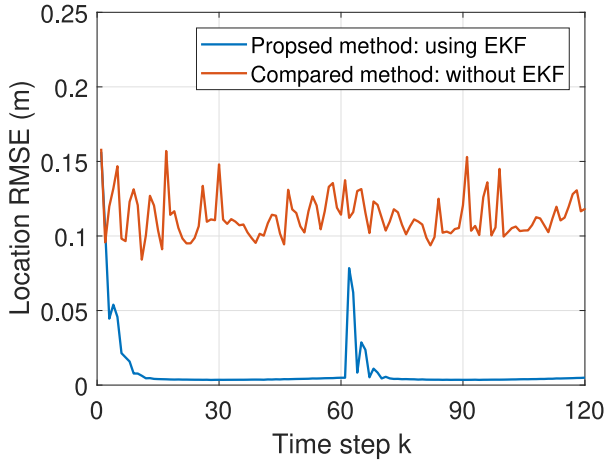

Fig. 5. Velocity process noise $\sigma_a^2 = 0.1$. Orientation process noise $\sigma_\alpha^2 = 0$. Comparison between the proposed method and the one without EKF.

requires 15 minutes. This significant difference highlights the much higher efficiency of the proposed method using EKF.

VI. Conclusion

We present a novel RIS-enabled passive localization and tracking use case, where a single-antenna full duplex transceiver transmits multiple OFDM signals and processes the signals reflected from the RIS-equipped object in a spectrum-efficient system. We demonstrate that the signals reflected by the RIS can be separated from the unknown and undesired multipath by using the designed RIS phase profile. Based on this, the location and velocity of the object can be estimated with proposed low-complexity estimators. Simulation results confirm that location estimation can achieve centimeter-level accuracy using only 6 MHz bandwidth.

Appendix

Since the state vector (13) is a real-valued vector, while the observation function (17) – (18) is a complex-valued vector, we write the Jacobian matrix as

$$\mathbf{H}_k \in \mathbb{R}^{L\times 5} = \begin{bmatrix} \frac{\partial \Re(\boldsymbol{h})}{\partial x} & \mathbf{0} & \frac{\partial \Re(\boldsymbol{h})}{\partial y} & \mathbf{0} & \frac{\partial \Re(\boldsymbol{h})}{\partial \alpha} \\ \frac{\partial \Im(\boldsymbol{h})}{\partial x} & \mathbf{0} & \frac{\partial \Im(\boldsymbol{h})}{\partial y} & \mathbf{0} & \frac{\partial \Im(\boldsymbol{h})}{\partial \alpha} \end{bmatrix}. \quad (25)$$

The function $\boldsymbol{h}$ at transmission l in (18) can be written as

$$\boldsymbol{h}(l) = N\sqrt{P_t}\rho_{0r}\sum_{m=1}^{M}\left(\cos\beta_{l,m} + j\sin\beta_{l,m}\right), \quad (26)$$

where $\beta_{l,m} = \boldsymbol{\omega}_{l,m} - \frac{4\pi}{\lambda} r_m \cos\varphi\cos(\theta-\alpha-\xi_m) + \psi$, such that the upper left entry in (25) becomes

$$\frac{\partial \Re(\boldsymbol{h}(l))}{\partial x} = \frac{\partial \Re(\boldsymbol{h}(l))}{\partial \varphi}\frac{\partial \varphi}{\partial x} + \frac{\partial \Re(\boldsymbol{h}(l))}{\partial \theta}\frac{\partial \theta}{\partial x}, \quad (27)$$

where

$$\begin{aligned} \frac{\partial \Re(\boldsymbol{h}(l))}{\partial \varphi} &= -N\sqrt{P_t}\rho_{0r}\frac{4\pi}{\lambda}\sin\varphi\sum_{m=1}^{M}\sin\beta_{l,m}r_m \\ &\quad\times\cos(\theta-\alpha-\xi_m), \\ \frac{\partial \Re(\boldsymbol{h}(l))}{\partial \theta} &= -N\sqrt{P_t}\rho_{0r}\frac{4\pi}{\lambda}\cos\varphi\sum_{m=1}^{M}\sin\beta_{l,m}r_m \\ &\quad\times\sin(\theta-\alpha-\xi_m), \\ \frac{\partial \varphi}{\partial x} &= \frac{-x\sin\varphi}{[\mathbf{p}_0]_3^2\cos\varphi}, \text{ and } \frac{\partial \theta}{\partial x} = \frac{-y}{x^2\left(1+\tan^2\theta\right)}. \end{aligned} \quad (28)$$

The calculation of the other entries in (25) follow similarly.

References

[1] Y. Liu et al., "Reconfigurable intelligent surfaces: Principles and opportunities," in *IEEE Commun. Surv. Tuts.*, vol. 23, no. 3, pp. 1546–1577, 3rd Quart., 2021.

[2] Z. Abu-Shaban, K. Keykhosravi, M. F. Keskin, G. C. Alexandropoulos, G. Seco-Granados, and H. Wymeersch, "Near-field localization with a reconfigurable intelligent surface acting as lens," in *Proc. IEEE Int. Conf. Commun.*, Montreal, QC, Canada, 2021, pp. 1–6.

[3] K. Keykhosravi, M. F. Keskin, G. Seco-Granados, and H. Wymeersch, "SISO RIS-enabled joint 3D downlink localization and synchronization," in *Proc. IEEE Int. Conf. Commun.*, Montreal, QC, Canada, 2021, pp. 1–6.

[4] K. Keykhosravi, M. F. Keskin, S. Dwivedi, G. Seco-Granados, and H. Wymeersch, "Semi-passive 3D positioning of multiple RIS-enabled users," *IEEE Trans. Veh. Technol.*, vol. 70, no. 10, pp. 11073–11077, Oct. 2021.

[5] R. Ghazalian, K. Keykhosravi, H. Chen, H. Wymeersch, and R. Jäntti, "Bi-static sensing for near-field RIS localization," in *Proc. IEEE Glob. Commun. Conf.*, Rio de Janeiro, Brazil, 2022, pp. 6457–6462.

[6] K. Keykhosravi, G. Seco-Granados, G. C. Alexandropoulos, and H. Wymeersch, "RIS-enabled self-localization: Leveraging controllable reflections with zero access points," in *Proc. IEEE Int. Conf. Commun.*, Seoul, South Korea, 2022, pp. 1–6.

[7] B. Teng, X. Yuan, R. Wang, and S. Jin, "Bayesian user tracking for reconfigurable intelligent surface aided mmwave mimo system," in *Proc. IEEE 12th Sensor Array Multichannel Signal Process. Workshop (SAM)*, Trondheim, Norway, 2022, pp. 201–205.

[8] S. Palmucci, A. Guerra, A. Abrardo, and D. Dardari, "Reconfigurable intelligent surfaces: A joint localization and communication perspective," in *Proc. IEEE 95th Veh. Technol. Conf. (VTC)*, Helsinki, Finland, 2022, pp. 1–5.

[9] M. Ammous and S. Valaee, "Positioning and tracking using reconfigurable intelligent surfaces and extended Kalman filter," in *Proc. IEEE 95th Veh. Technol. Conf. (VTC)*, Helsinki, Finland, 2022, pp. 1–6.

[10] S. W. Ellingson, "Path loss in reconfigurable intelligent surface-enabled channels," in *Proc. IEEE 32nd Annu. Int. Symp. Pers., Indoor Mobile Radio Commun. (PIMRC)*, Helsinki, Finland, 2021, pp. 829–835.

[11] Z. Ye, F. Junaid, R. Nilsson, and J. Van De Beek, "Single-antenna sensor localization with reconfigurable intelligent surfaces," in *Proc. IEEE Glob. Commun. Conf.*, Rio de Janeiro, Brazil, 2022, pp. 6200–6205.

[12] L. Hong, "Discrete constant-velocity-equivalent multirate models for target tracking," *Math. Comput. Model.*, vol. 28, no. 11, pp. 7–18, 1998.

[13] G. F. Basso, T. G. Silva De Amorim, A. V. Brito, and T. P. Nascimento, "Kalman filter with dynamical setting of optimal process noise covariance," *IEEE Access*, vol. 5, pp. 8385–8393, 2017.